A MODEL FOR MOISTURE-CONTENT EVOLUTION IN POROUS BUILDING ELEMENTS: TREATMENT OF IRREGULAR REGIONS

Regina Katsman ,
NRC/IRC, Bld. M-24, Montreal Rd., Ottawa
ON K1A 0R6, Canada

Regina.Katsman@nrc.ca

Rachel Becker
Department of Civil Engineering, Technion
Israel Institute of Technology, Haifa, 32000,
Israel

Becker@tx.technion.ac.il

ABSTRACT

The effects of moisture movement and residual moisture content are becoming a recognized part of a performance based design of buildings. Despite the long-time existence of a basic 3-D formulation of heat and mass transfer within porous materials, the generalized hygrothermal behavior of construction elements that contain hygrothermal bridges and/or air voids has not been studied. Neither have the processes, which occur at the interfaces between different materials, been investigated. Relying on basic energy and mass conservation principles, a general integral form of presentation was applied to establish the coupled heat and mass transfer field equations, which were further transformed to a discrete set of algebraic equations. This form of presentation is more suitable for treatment of irregular regions, such as material interfaces and internal air voids. To treat these regions, specific mathematical procedures were implemented. Two Software packages were written to simulate the evolution of moisture content in non-homogeneous flat planar walls, without and with air voids. Finally, the results of modeling are presented for both types of constructions, thus enabling one to analyse a hygrothermal behavior of irregular wall's regions.

INTRODUCTION

For most planar building elements (usually designated by the general term walls), the main moisture movement is in the direction perpendicular to the element's air-exposed surfaces. However, the non-homogeneous structure of the element within its main plane causes multidirectional moisture movement. The general formulation of simultaneous heat and mass transfer in a porous material has been performed by Luikov [1] in order to analyze moisture transport phenomena in soils. It has then been implemented for building materials by Philip and De-Vries [2] and since then by others [3,4]. The field equations, which emerge from this formulation, have been used since then for analyzing various cases. These works include investigations of 1-D heat and mass transfer phenomena in building elements composed of a homogenous building material [4 to 9]. Despite the long-time existence of a basic 3-D formulation of heat and mass transfer within porous materials, the generalized hygrothermal behavior of construction elements that contain hygrothermal bridges and air voids has not been studied yet. Neither have the processes, which occur at the interfaces between different materials, been investigated. Moreover, the effects of commonly existing air-voids (in the form of large hollow-cores or small deffects) within the materials composing the wall, or at the interfaces between the materials (as usually stems from the construction methods for the jointing), have not been studied either.

This paper is devoted to the mathematical modeling and numerical solution of the moisture-content evolution in walls with hygrothermal bridges, including the case of a construction with air voids, concentrating mainly on methods of mathematical treatment of irregular wall's regions.

MATHEMATICAL MODEL

The basic physical considerations and previous research indicate that the mutual influence of the heat and mass transfer is an inherent property of the explored system. Moreover, the mutual influence of these phenomena on the moisture-content evolution may be particularly significant at the boundaries, where solid meets humid air with variable humidity, and at interfacial zones between different materials.

Generally, the above-mentioned Philip and De-Vries differential equations are actually an outcome of the energy and mass conservation principles. However, for the present aims, the integral form of presenting these basic priciples is the most suitable, as it enables easy inclusion of interfaces between different materials, internal air-voids and their internal boundaries.

General Scheme

The heat and mass field equations at every material point are derived from the basic energy and mass conservation principles:

$$Q_S = Q_I + Q_T + Q_v \qquad (1)$$

$$E_S = E_I + E_T + E_W \tag{2}$$

Where:

Q_S is the heat stored in an arbitrary control-volume V (with a total surface area S) during the time interval dt

Q_T is the total resultant in-flowing heat across S caused by the temperature gradient ∂T/∂n (at the surface, with the normal n to S pointing outwards at every point on S)

Q_I is the total resultant heat produced within the volume V by internal heat sources and sinks (e.g. due to heat of hydration of cementitious compounds)

Q_v is the total resultant in-flowing latent heat (associated with vaporization and condensation processes) across S, caused by the partial water-vapor pressure gradient ∂p/∂n (at the surface, with the normal n as above)

E_S is the total moisture stored in the same volume V during the time interval dt

E_I is the total resultant moisture produced within the volume V by internal moisture sources and sinks (e.g. due to the hydration process of cementitious materials)

E_T is the total resultant in-flowing moisture across S caused by the temperature gradient

E_W is the total resultant in-flowing moisture across S caused by the moisture-gradient ∂W/∂n (at the surface, with the normal n as above).

For the case without internal sources or sinks, delineation of each factor then yields the following integral presentations:

$$Q_S = \int_{t_1}^{t_2} dt \cdot \iiint_V c \cdot \rho \cdot \frac{\partial T}{\partial t} \cdot dV \tag{3}$$

$$Q_T = \int_{t_1}^{t_2} dt \cdot \iint_S \lambda \cdot \frac{\partial T}{\partial n} \cdot dS \tag{4}$$

$$Q_v = \int_{t_1}^{t_2} dt \cdot \iint_S L \cdot D_v \cdot \frac{\partial p}{\partial n} \cdot dS \tag{5}$$

$$E_S = \int_{t_1}^{t_2} dt \cdot \iiint_V \frac{\partial W}{\partial t} \cdot dV \tag{6}$$

$$E_T = \int_{t_1}^{t_2} dt \cdot \iint_S D_T \cdot \frac{\partial T}{\partial n} \cdot dS \tag{7}$$

$$E_W = \int_{t_1}^{t_2} dt \cdot \iint_S D_W \cdot \frac{\partial W}{\partial n} \cdot dS \tag{8}$$

Conducting several transformations, the field equations are thus given by:

$$\int_{t_1}^{t_2} dt \cdot \iiint_V c \cdot \rho \cdot \frac{\partial T}{\partial t} \cdot dV = \int_{t_1}^{t_2} dt \cdot \iint_S \lambda \cdot \frac{\partial T}{\partial n} \cdot dS + \int_{t_1}^{t_2} dt \cdot \iint_S L \cdot D_{vT} \cdot \frac{\partial T}{\partial n} \cdot dS + \int_{t_1}^{t_2} dt \cdot \iint_S L \cdot D_{vW} \cdot \frac{\partial W}{\partial n} \cdot dS \tag{9}$$

$$\int_{t_1}^{t_2} dt \cdot \iiint_V \frac{\partial W}{\partial t} \cdot dV = \int_{t_1}^{t_2} dt \cdot \iint_S D_W \cdot \frac{\partial W}{\partial n} \cdot dS + \int_{t_1}^{t_2} dt \cdot \iint_S D_T \cdot \frac{\partial T}{\partial n} \cdot dS \tag{10}$$

The system of partial differential equations for the simultaneous heat and mass transfer at a regular point within the porous material, which is obtained from the integral equations 9 and 10 when $V \to 0$, corresponds to the classical Philip and De-Vries formulations and to those given by the IEA Annex 24. However, as presented in the following sections, the integral presentation is more suitable for the general development of the equations in irregular regions, such as material interfaces and internal voids. Moreover, it is more amenable for establishing the numerical integration procedures at irregularities and at all the internal and external boundary points.

Analytical Treatment of Irregular Regions

The following continuity equations emerge at materials' interfaces when the zero-limit is reached for two infinitesimal control volumes that have a mutual interface S:

$$T\big|_{-S} = T\big|_{+S} \tag{11}$$

$$p\big|_{-S} = p\big|_{+S} \tag{12}$$

$$
\begin{aligned}
&[\int_{t_1}^{t_2} dt \iint_S (\lambda + L \cdot D_{vT}) \frac{\partial T}{\partial n} dS \\
&+ \int_{t_1}^{t_2} dt \iint_S L \cdot D_{vW} \cdot \frac{\partial W}{\partial n} dS]\Big|_{-S} \\
&+ [\int_{t_1}^{t_2} dt \iint_S (\lambda + L \cdot D_{vT}) \frac{\partial T}{\partial n} dS \\
&+ \int_{t_1}^{t_2} dt \iint_S L \cdot D_{vW} \cdot \frac{\partial W}{\partial n} dS]\Big|_{+S} = 0
\end{aligned}
\qquad (13)
$$

$$
\begin{aligned}
&[\int_{t_1}^{t_2} dt \iint_S D_W \cdot \frac{\partial W}{\partial n} dS + \\
&\int_{t_1}^{t_2} dt \iint_S D_T \cdot \frac{\partial T}{\partial n} dS]\Big|_{-S} + \\
&[\int_{t_1}^{t_2} dt \iint_S D_W \cdot \frac{\partial W}{\partial n} dS + \\
&\int_{t_1}^{t_2} dt \iint_S D_T \cdot \frac{\partial T}{\partial n} dS]\Big|_{+S} = 0
\end{aligned}
\qquad (14)
$$

The following boundary-condition equations emerge at material-air boundaries when the zero-limit is reached for an infinitesimal control volume with an air-exposed surface S:

$$
\begin{aligned}
&\int_{t_1}^{t_2} dt \iint_S h_s dT_{aS} dS + \\
&\int_{t_1}^{t_2} dt \iint_S (\lambda + L \cdot D_{vT}) \cdot \frac{\partial T}{\partial n} dS + \\
&\int_{t_1}^{t_2} dt \iint_S L \cdot D_{vW} \cdot \frac{\partial W}{\partial n} dS = 0
\end{aligned}
\qquad (15)
$$

$$
\begin{aligned}
&\int_{t_1}^{t_2} dt \iint_S \beta_s \cdot dp_{aS} \cdot dS + \\
&\int_{t_1}^{t_2} dt \iint_S D_W \cdot \frac{\partial W}{\partial n} \cdot dS + \\
&\int_{t_1}^{t_2} dt \iint_S D_T \cdot \frac{\partial T}{\partial n} \cdot dS = 0
\end{aligned}
\qquad (16)
$$

Derivation of the equations for an element with air-voids is now straightforward. Figure 1 depicts the schemes for the relevant control volumes within the regular porous material (Volume 1) and within the air-void (Volume 2).

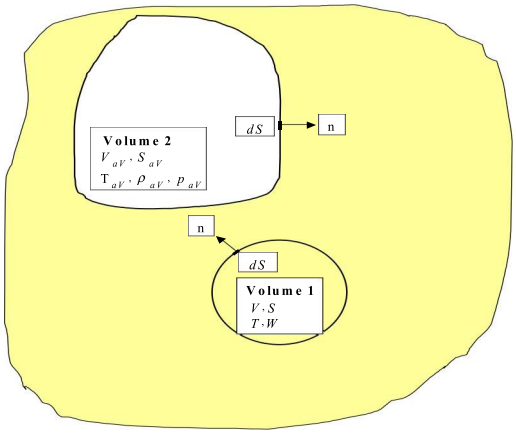

Figure 1: Scheme of general control-volumes within the element's regular material region (Volume 1) and an air-void (Volume 2).

As a first order approximation, it is assumed that within the void the air temperature and partial water-vapor pressure distributions are uniform, except for an extremely thin boundary layer at the interface with the surrounding solid. Thus, across the void the temperature and partial water-vapor pressure are represented by unique values, T_{aV} and p_{aV}. Wherever part of the solid material continuum is replaced by an air-void, equations 9 and 10 re-written for the total entrained air volume V_{aV} that is bounded by the surface S_{aV} (with a normal n into the porous medium). After substitution of 15 and 16 this yields:

$$
\begin{aligned}
&V_{aV} \cdot \int_{t_1}^{t_2} c_{aV} \cdot \rho_{aV} \cdot \frac{\partial T_{aV}}{\partial t} \cdot dt = \\
&\int_{t_1}^{t_2} dt \cdot \iint_{S_{aV}} \lambda \cdot \frac{\partial T}{\partial n} \cdot dS + \int_{t_1}^{t_2} dt \cdot \iint_{S_{aV}} L \cdot D_{vT} \cdot \frac{\partial T}{\partial n} \cdot dS + \\
&\int_{t_1}^{t_2} dt \cdot \iint_{S_{aV}} L \cdot D_{vW} \cdot \frac{\partial W}{\partial n} \cdot dS = -\int_{t_1}^{t_2} dt \iint_{S_{aV}} h_{s_{aV}} dT_{aS} dS
\end{aligned}
\qquad (17)
$$

$$V_{aV}\cdot\int_{t_1}^{t_2}\frac{\partial\rho_{aV}}{\partial t}dt=\int_{t_1}^{t_2}dt\cdot\iint_{S_{aV}}D_W\cdot\frac{\partial W}{\partial n}\cdot dS+$$

$$\int_{t_1}^{t_2}dt\cdot\iint_{S_{aV}}D_T\cdot\frac{\partial T}{\partial n}\cdot dS=$$

$$-\int_{t_1}^{t_2}dt\iint_{S_{aV}}\beta_{s_{aV}}\cdot dp_{aS}\cdot dS \qquad (18)$$

This model does not take into account gravitational moisture movement that occurs in pores or cracks outside the capillary range, or within vertical air-voids. Neither does it address the convection inside the porous material, effects of direct rainfall, solar radiation or air transport.

NUMERICAL SOLUTION

General Scheme

The solution procedure adopted here is based on the presentation of the integral equations in a discrete form, including the boundaries and air-voids. An implicit scheme was chosen for the numerical integration process. The ensuing discrete set of algebraic equations with non-constant coefficients is solved by means of an iterative convergence process. In addition, at this stage the solution was limited to the case of an orthogonal x-y coordinate system, as most building walls have only orthogonal internal and external surfaces.

Using an implicit scheme for the linearized set of equations provides the stability of the numerical solution without dependence on time and space steps. In particular, for the iterative process used to solve the equations with variable coefficients this scheme is preferred because of its monotonous behavior. The examples presented in this paper were solved using the "optimal" time steps that stem from the spatial mesh, which was chosen in accordance with the geometric features of the analyzed construction, where the term "optimal" refers in this case to the time step that would be recommended as maximal in order to render an explicit scheme stable (i.e. $\Delta t_{\max}=\min[(dn)^2/(2\cdot\alpha)]$, where dn designates a mesh step in any direction and α any of the relevant diffusivity coefficients in the equations).

The scheme for the numerical model is shown in Figure 2.

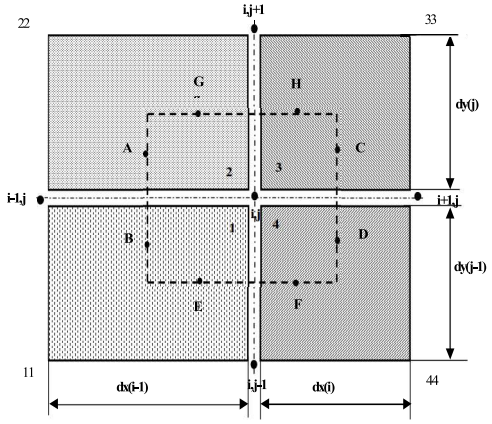

Figure 2: Scheme of the mesh at a general point i,j.

The integration points (nodes i,j) are on an orthogonal grid, with main grid line along all material boundaries. The grid is composed between its main lines by a variable-size mesh. The control volume around every node extends until the mid-distance to the next mesh-node in every direction (rectangle ABEFDCHG in Figure 2). Each of the four parts of the control volume, 1 to 4, may be composed of a different material.

Numerical Treatment of Irregular Regions

In establishing the field and boundary condition equations, the temperature and moisture content within each part are presented by their values at the node i,j. If at a certain node nm different materials meet (nm≤4), moisture-content in these materials at the node, $W_{i,j}^k$ (k=1,…,nm), is different, while the temperature, $T_{i,j}$, and the partial water-vapor pressure, $p_{i,j}$, are identical (i.e. Relative-Humidity values, $\varphi_{i,j}$, are also identical).

The different moisture-contents at the node, generally presented by the four points 1 to 4, are inter-dependent. Their dependence is obtained via the sorption isotherms of the different materials. The following procedure was used for instantaneous linearization of the discrete set of equations: At every iteration-step, m, undertaken within a given time step, dt^n, from n to n+1 (with n=0 at t=0):

$$\left(\frac{\partial W_{i,j}^k}{\partial t}\right)^{n+1}=\left(\frac{\partial W_{i,j}^k}{\partial W_{i,j}^1}\right)^m\cdot\left(\frac{\partial W_{i,j}^1}{\partial t}\right)^{n+1}=$$

$$\left(\frac{\partial W_{i,j}^k}{\partial\varphi}\cdot\frac{\partial\varphi}{\partial W_{i,j}^1}\right)^m\cdot\left(\frac{\partial W_{i,j}^1}{\partial t}\right)^{n+1}=$$

$$(\frac{\xi_{i,j}^{k}}{\xi_{i,j}^{1}})^{m} \cdot (\frac{\partial W_{i,j}^{1}}{\partial t})^{n+1} \tag{19}$$

for k that runs from 2 to 4.
Or, re-written in the discrete form:

$$(W_{i,j}^{k})^{n+1} = (W_{i,j}^{k})^{n} + (\frac{\xi_{i,j}^{k}}{\xi_{i,j}^{1}})^{m} \cdot ((W_{i,j}^{1})^{n+1} - (W_{i,j}^{1})^{n}) \tag{20}$$

For the sake of brevity, $(W_{i,j}^{1})^{n}$ and $(W_{i,j}^{1})^{n+1}$ are denoted in the sequel by $W_{i,j}^{n}$ and $W_{i,j}^{n+1}$.
For equations at internal and external boundaries, the values of $p_{i,j}^{n+1}$ are unknowns. They depend, however, non-linearly on the unknowns $T_{i,j}^{n+1}$ and $W_{i,j}^{n+1}$. Disceretization and linearization are thus performed by the following:

$$p_{i,j}^{n+1}(T_{i,j}^{n+1}, W_{i,j}^{n+1}) = p_{i,j}^{n}(T_{i,j}^{n}, W_{i,j}^{n}) + fs_{i,j}^{m} \cdot (T_{i,j}^{n+1} - T_{i,j}^{n}) + gs_{i,j}^{m} \cdot (W_{i,j}^{n+1} - W_{i,j}^{n}) \tag{21}$$

Where:

$$p_{i,j}^{n}(T_{i,j}^{n}, W_{i,j}^{n}) = p_{sat,i,j}^{n}(T_{i,j}^{n}) \cdot \varphi_{i,j}^{n}(T_{i,j}^{n}, W_{i,j}^{n}), \tag{22}$$

$$fs_{i,j}^{m} = (\frac{\partial p_{i,j}}{\partial T_{i,j}})^{m} \tag{23}$$

$$gs_{i,j}^{m} = (\frac{\partial p_{i,j}}{\partial W_{i,j}})^{m} = \frac{p_{sat,i,j}^{m}}{\xi_{i,j}^{m}} \tag{24}$$

The local instantaneous values of all the terms on the RHS of equations 23 and 24, at the intermediate time step m, are thus derived from the local instantaneous values $T_{i,j}^{m}$ and $W_{i,j}^{m}$. These parameters are further calculated by means of additional inherent series of sub-iterations applied for each iterative convergence stage, from time step n to n+1.
Two Software packages, MA2DW and MA2DWV, were written to solve numerically the evolution of moisture content in flat planar walls and verified by specific examples. The first one is designed for the solution of walls without air voids and the second for those with.

EXAMPLES

Two examples are given to demonstrate the effects occurring in the irregular regions that are highlighted by the suggested 2-D analysis for a drying process of a block-wall with joints and surface-renderings. These examples are restricted to the case of a symmetrical AAC wall with cementitous-mortar joints and renderings, without and with air-voids, drying symmetrically from a nearly saturated initial state.

Construction data

The element without air-voids is shown in Figure 3,

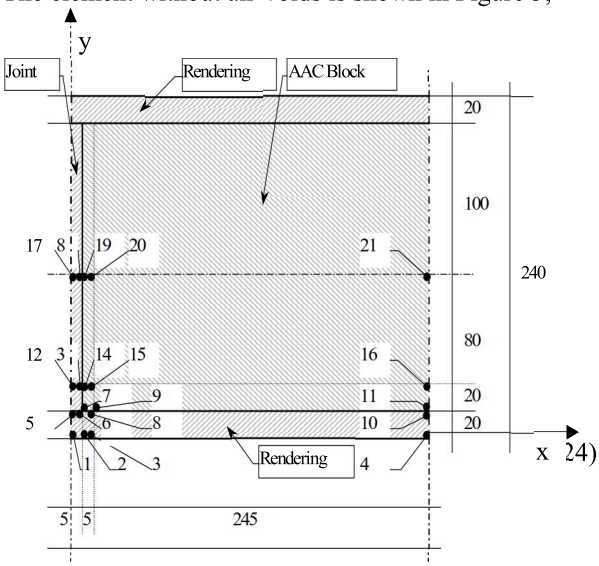

Figure 3: The element without air-voids.

while the one with air-voids is depicted in Figure 4.

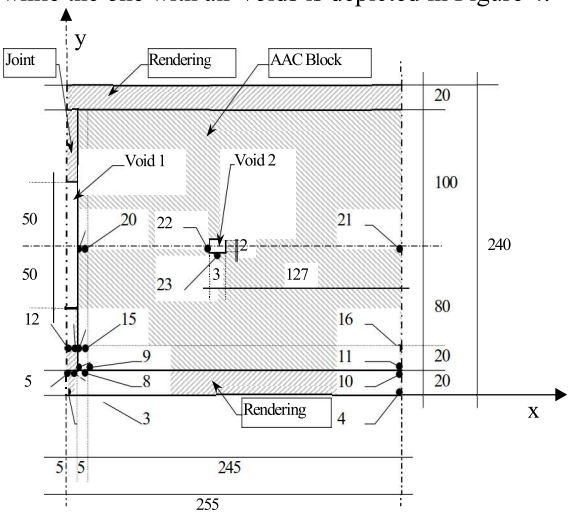

Figure 4: The element with air-voids.

Air-void No. 1 represents a cavity in the joint-mortar in accordance with the manner of construction frequently adopted for block-walls. Air-void No. 2 represents a

$$x\ 24) \tag{32}$$

small defect in the block. The numbered points depict the locations of results presented in various following figures.

According to accumulated test data [10,12] the moisture-dependence of the water-vapor permeability, moisture diffusivity and thermal conductivity of cementitious materials are given by:

$$D_v = D_{vd} + A_1 \cdot \varphi^{A_2} \quad (25)$$

$$D_W = D_{Wd} \cdot \exp(C_1 \cdot W) \quad (26)$$

$$\lambda = \lambda_d (1 + D_1 \cdot W) \quad (27)$$

Where:

$D_{vd}, D_{Wd}, \lambda_d$ are the relevant properties of the dry material (assuming they do not depend on temperature), and

A_1, A_2, C_1, D_1 are constant coefficients (assuming they do not depend on temperature).

The material data used in these runs represent an AAC block and a cementitious-mortar, with dry densities of 510 and 1822 kg/m^3 respectively, and a common specific heat capacity of 840 $J/(kg \cdot C)$. The mortar's water-vapor permeability is a little smaller than the block's (their ratio changes from ≈3/4 when dry to ≈1/3 when wet), whereas its moisture diffusivity is approximately 15 times larger.

Surface coefficients utilized on the airside surfaces (for both sides of the construction) were [14]:

$$h_S = 8.33 \frac{W}{m^2 \cdot C}, \ \beta_S = 2.6 \cdot 10^{-8} \frac{s}{m}$$

Surface coefficients within the air-void were [14]:

$$h_{S_{aV}} = 4.543 \frac{W}{m^2 \cdot C}, \ \beta_{S_{aV}} = 2.53 \cdot 10^{-8} \frac{s}{m}$$

Initial and boundary conditions

The initial conditions in all materials correspond to the following values:

$T(0) = 20°C$, $\varphi(x,0) = 95\%$.

With moisture content established according to the sorption isotherm.

The drying process is initiated by a drop in the relative humidity of the air adjacent to both surfaces to 42%, while the temperature remains constant.

Analysis and discussion of results

Figures 5 to 6 present results of the analysis for the element without air-voids, while Figures 7 to 9 present results for the element with the two air-voids.

The element without air-voids

Figure 5 presents moisture-content distributions for the whole cross-section after a period of 1350 hours.

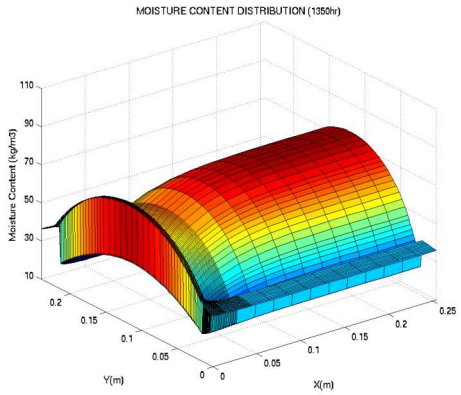

Figure 5: Results for the element without air-voids. Moisture-content distributions after 1350 hours.

Figure 6 presents the evolution of the drying process at points 5 to 11, located at the Block-Mortar intersection (Figure 3).

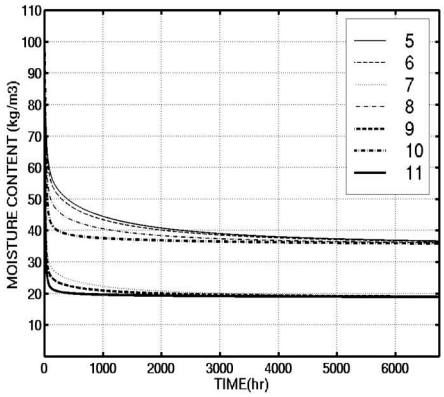

Figure 6: Results for the element without air voids. Moisture-content evolutions at various points within the cross-section.

One can see that, as expected, at the finite state of the drying process moisture contents in the various materials correspond eventually to their sorption isotherms, without dependence on the process that they undergo. The drying pattern of the block is highly influenced by the mortar surrounding it. While the inner part of the block dries extremely slowly (Figure 5), the drying process at points closer to the mortar (joint and renderings) is much faster, with point 11 drying the fastest, and points 9 and 7 only a little slower (Figure 6). These results indicate that the large moisture diffusivity of the mortar is in this case the main cause for the faster drying processes within itself and within

the block material in its vicinity. On the other hand, the smaller moisture diffusivity of the block material does not affect the rate of drying of the rendering (points 5, 6, 8, and 10). Due to the passage of moisture from the blocks into the joint, all along their interfaces, points 5 and 6 in the mortar dry a little slower than point 8.

The element with air-voids

Figure 7 presents moisture-contents distributions throughout the whole cross-section after a period of 1350 hours.

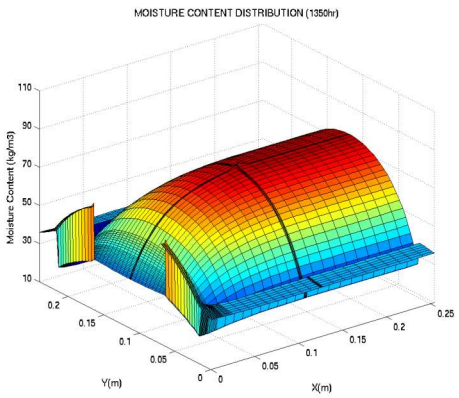

Figure 7: Results for the element with air-voids. Moisture-content distributions after 1350 hours.

Only differences stemming from the presence of the air-voids are discussed.

The substitution of joint mortar by an air-void cuts off the moisture transport by liquid water and enables only vapor transport via the void. The small air-void within the block has obviously only a local effect. The decrease in partial water-vapor pressure and relative-humidity within this void is very slow, thus slowing down even further the drying rate of points 22, 23 in comparison to point 21 all along the drying process (Figure 8).

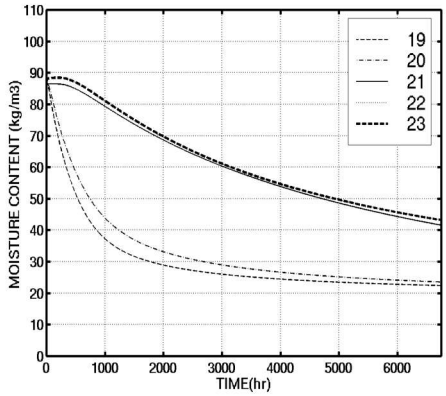

Figure 8: Results for the element without air-voids. Moisture-content evolutions at various points within the cross-section.

The results show that the partial water-vapor pressure in the large void decreases much faster than that in the small one (Figure 9).

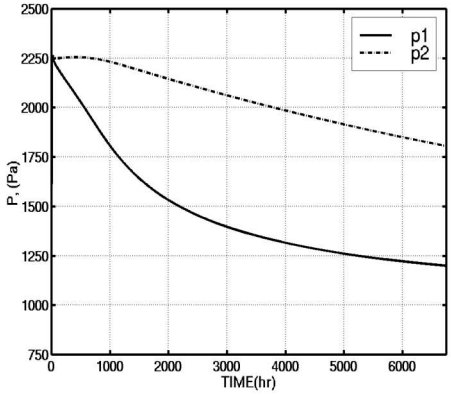

Figure 9: Results for the element with air voids. Partial water-vapor pressure within the two air-voids.

Point 19 exhibits, thus, generically similar behavior to that of points 22 and 23, but quantitatively much less pronounced (Figure 8).

CONCLUSIONS

The paper presents a tool developed for the simulation of moisture evolution in masonry walls, based on the coupled hygrothermal behavior of porous materials.

The 3-D integral form of presentation was used to allow easy inclusion of interfaces between different materials, internal air-voids and their internal boundaries.

The presented numerical procedure has ensured an accurate treatment of the irregular regions.

The developed computer Software packages were designed to allow the analysis of 2-D moisture-content evolution in non-homogeneous building constructions.

To provide analysis of the hygrothermal behavior of the irregular regions, included within real building wall, two examples were exhibited. The wall under analysis was constructed from AAC blocks and cementitious mortar.

Results indicate the severe impact of the mortar's relatively high moisture diffusivity on the processes occurred in other materials in mortar's vicinity. An impact of air voids is estimated to be a local one.

NOMENCLATURE

B_n - Sorption isotherm coefficients

c - Specific heat capacity, $(J/(kg \cdot C))$

h_s - Heat transfer surface coefficient, $(W/(m^2 \cdot C))$

D_T -Thermal moisture diffusion coefficient of the material, $(kg/(m \cdot s \cdot C))$

D_v -Water-vapor permeability coupled to the partial water-vapor pressure gradient, (s)

D_{vT} -Thermal water-vapor diffusion coefficient of the material, $(kg/(m \cdot s \cdot C))$

D_{vW} -Diffusivity of water-vapor coupled to the moisture pressure gradient, (m^2/s)

D_W -Moisture diffusivity, (m^2/s)

L - Latent heat of water-vaporization, (J/kg)

n -Perpendicular to a surface, pointing outwards of control-volume (m)

p -Partial water-vapor pressure, (Pa)

P_a -Absolute air-pressure, (Pa)

p_s -Partial water-vapor pressure at the surface, (Pa)

p_{sat} -Partial water-vapor pressure at saturation, (Pa)

S -Surface, (m^2)

t -Time, (s)

T -Temperature, (C)

T_a -Air temperature, (C)

T_g -Temperature of the reference sorption isotherm for a given material, (C)

T_s -Surface temperature, (C)

V -Control-volume, (m^3)

V_{aV} -Air-void volume, (m^3)

W -Moisture-content, (kg/m^3)

Greek symbols

β_s -Water-vapor transfer surface coefficient, (s/m)

λ -Thermal conductivity, $(W/(m \cdot C))$

ρ -Density, (kg/m^3)

ρ_a -Air density, (kg/m^3)

φ -Relative humidity,

REFERENCES

1. Luikov, A.V. (1966), Heat and mass transfer in capillary-porous bodies. Pergamon Press, (in Russian).
2. de Vries, D.A. (1958), Simultaneous transfer of heat and moisture in porous media. Transactions, American Geophysical Union, Vol. 39, No.5.
3. Andersson, A.C. (1985), Verification of calculation methods for moisture transport in porous building materials. Swedish Council for Building Research, D6.
4. Hens, H. (1996), Heat, air and moisture transfer in insulated envelope parts, Task 1: modeling. International Energy Agency (IEA), Annex 24, Final Report, Volume 1.
5. Burch, D. (1997), MOIST, APC program for predicting heat and moisture transfer in building envelopes. Building and Fire Research Laboratory, NIST, Special Publication 917.
6. Van Der Kooi, J. (1971), Moisture transport in cellular concrete roofs. Ph.D. thesis. Delft. Waltman.
7. Brocken, H.J.P. and Smolders, H.R. (1997), Moisture transport over the brick-mortar interface: water absorption and drying. Heat and Moisture Transfer in Buildings, CIB Proceedings, Publications 213, 1:249-258.
8. de Freitas, V.P. (1993), The moisture migration in building walls, experimental and analytical study. CIB W40 report, pp.1-15.
9. Bomberg, M. (1974), Moisture flow through porous building materials. Report No. 52, Lund Institute of Technology. Lund.
10. Kumar Kumaran, M. (1996), Heat, air and moisture transfer in insulated envelope parts, Task 3: material properties. International Energy Agency (IEA), Annex 24, Final Report Volume 3.
11. Hansen, K.K. (1986), Sorption isotherms, a catalogue. The Technical University of Denmark, Department of Civil Engineering, Building Materials Laboratory.
12. IEA-ANNEX XIV (1991), Condensation and energy, material properties. International Energy Agency (IEA), Annex XIV Report, Vol. 3.
13. Descamps, F. and Hens, H. (1992) Test of the diffusion approach to capillary water transfer in porous building materials, Katholieke Universiteit Leuven, pp.1-50.
14. Billington, S.N. (1967), Building physics: heat. Pergamon Press LTD.